


Establishment of a Zebrafish Xenograft Model for *in Vivo* Investigation of Nasopharyngeal Carcinoma

Cell Transplantation
Volume 31: 1–12
© The Author(s) 2022
Article reuse guidelines:
sagepub.com/journals-permissions
DOI: 10.1177/09636897221116085
journals.sagepub.com/home/cll


Enyu Huang^{1,2}, Haofeng Huang¹, Longji Wu², Binbin Li²,
Zhiwei He², and Jingjing Zhang^{1,3} 

Abstract

Nasopharyngeal carcinoma (NPC) is a unique malignant tumor of the head and neck. Despite higher survival rates by the combination of radiotherapy and chemotherapy, the recurrence or metastasis of NPC still occurs at about 10%. Therefore, there is urgent demand to develop more effective *in vivo* models for preclinical trials to investigate the mechanisms of NPC development and progression and to explore better treatment approaches. In this study, we transplanted human NPC CNE1 cells into zebrafish embryos to establish a xenograft model of NPC, where the proliferation and invasion behaviors of NPC cells were investigated *in vivo*. Combining *in vitro* and *in vivo* analyses, we found that activating transcription factor 7 (ATF7) was involved in the occurrence and development of NPC regulated by peptidyl-prolyl *cis-trans* isomerase NIMA-interacting 1 (Pin1). The zebrafish NPC xenograft model established here thereby provides an *in vivo* tool for exploring the occurrence and development of NPC, which may help to identify new tumor markers and develop new therapeutic strategies for the treatment of NPC.

Keywords

zebrafish, nasopharyngeal carcinoma, xenograft, Pin1, ATF7

Introduction

Nasopharyngeal carcinoma (NPC) is a unique head and neck malignant tumor, which originates from nasopharyngeal epithelium. It is one of the malignant tumors with high incidence rate in South China and Southeast Asian countries^{1,2}. Studies have shown that the occurrence of NPC is related to Epstein-Barr virus (EBV) infection, genetic susceptibility, and environment². Due to the special anatomical location and high radiosensitivity of NPC, current main treatment method of NPC is to combine radiotherapy and chemotherapy^{3,4}. Although it has a higher survival rate, the recurrence or metastasis rate of NPC is about 10% in patients received radiotherapy combined with chemotherapy^{5,6}. In addition, chemotherapy resistance is usually accompanied by a poor prognosis, which is also a major obstacle for the treatment of patients with recurrent NPC. Therefore, to improve the survival rate of patients is still a major challenge in the treatment of NPC. There are urgent needs to develop more effective *in vivo* NPC models for preclinical trials, so as to explore the mechanisms involved in NPC occurrence and progression.

Model organisms are important for studying and understanding human diseases. Traditional vertebrate models include mice, rats, and so on. Among them, mouse is the most widely used model to establish xenotransplantation models for evaluating the preclinical efficacy of anticarcinogen⁷.

Despite the increase of various immunodeficient and humanized mouse models, there are still inherent limitations with these models. For example, mice are not suitable for large-scale screening of small molecules due to their high cost, long life cycle, and large breeding space needed. In addition, it is difficult to intravitaly image internal cancers in mice. To complement these shortages in mice models, zebrafish xenograft models were developed. Zebrafish has very conserved genome compared with human and owns highly homologous

¹ Affiliated Hospital of Guangdong Medical University & Key Laboratory of Zebrafish Model for Development and Disease of Guangdong Medical University, Zhanjiang, China

² China-American Cancer Research Institute, Guangdong Medical University, Dongguan, China

³ The Marine Biomedical Research Institute of Guangdong Zhanjiang, Zhanjiang, China

Submitted: January 24, 2022. Revised: July 2, 2022. Accepted: July 4, 2022.

Corresponding Authors:

Jingjing Zhang, Affiliated Hospital of Guangdong Medical University & Key Laboratory of Zebrafish Model for Development and Disease of Guangdong Medical University, Zhanjiang 524001, China.
Email: jingjing.zhang@live.com

Zhiwei He, China-America Cancer Research Institute, Guangdong Medical University, Dongguan 523808, China.
Email: hezhiwei@gdmu.edu.cn



oncogenes and tumor suppressor genes, making it an ideal model for identifying carcinoma-related genes and screening therapeutic compounds⁸. Furthermore, zebrafish has already been shown as a suitable animal model for studying the pathological mechanisms of many diseases due to its availability, operability, transparent body, and low cost^{9,10}. Most importantly, its adaptive immune system does not mature until 4 weeks after fertilization^{11,12}. Xenograft models establishment in zebrafish embryos can avoid immune rejection efficiently. Moreover, by combining the fluorescent labeling of tumor cells, the transparent fish body allows to access and trace the transplanted cells *in vivo* in single-cell resolutions, and to observe the migration of tumor cells and the formation and metastasis of tumors by imaging time-lapse movies¹³.

In this study, we aimed to establish a zebrafish NPC xenograft model to provide an *in vivo* system to investigate the migration and invasion of NPC cells and also the formation of NPC *in vivo*. Meanwhile, the role of the peptidyl-prolyl *cis-trans* isomerase NIMA-interacting 1 (Pin1) on the NPC formation and on the regulation of the activating transcription factor 7 (ATF7) was investigated using this *in vivo* model. The results indicated that the zebrafish xenograft model could be an efficient model system for studying the tumorigenesis and the progress of NPC *in vivo*.

Materials and Methods

Cell Culture and Transfection

The NPC CNE1 cells were cultured in RPMI 1640 medium (Gibco, Thermo Fisher Scientific) supplemented with 10% fetal bovine serum (FBS; Thermo Fisher Scientific, Waltham, MA, USA) at 37°C in a humidified chamber containing 5% CO₂. For establishment of CNE1-LV3 and CNE1-*shPin1* cells, CNE1 cells were sequentially infected with LV3 and *shPin1* lentiviral particles (the lentivirus packaging vector of *pGLV3/H1/GFP* was purchased from GenePharma Co., Ltd, Suzhou, China) using polybrene transfection enhancer (Sigma-Aldrich, Darmstadt, Germany) and screened with 1 µg/ml puromycin. *Pin1* shRNA sense: 5'-GCTCAGGCCG AGTGTACTA-3' and antisense: 5'-TAGTACACTCGGCCT GAGC-3'. The plasmids used in this experiment were constructed previously in our group¹⁴. A total of 5 × 10⁴ CNE1 cells were seeded to a 6-well plate 24 h before transfection. *Pin1* overexpression vector or negative control vector was mixed together with lipofectamine 2000 for transfection when the cells were at a 60% to 70% confluence. Cells were harvested for protein extraction at 36–48 h after transfection.

Zebrafish Husbandry

Wild-type zebrafish AB and transgenic zebrafish *Tg(kdrl:mCherry)* were kept according to standard laboratory procedures^{15,16}. Adult zebrafish were raised in a circulatory system at 28.5°C for 14 h of light and 10 h of darkness¹⁷. For

zebrafish mating, sexually mature zebrafish were placed in pairs in the mating tank overnight, and the following day, they begin spawning when the light is on. Embryos were collected, rinsed, and placed in Petri dishes containing embryo water. Embryos were incubated in an incubator at 28.5°C. To prevent pigment formation in larvae, 0.003% (w/v) phenylthiocarbamide/*N*-phenylthiourea (PTU; Sigma-Aldrich) was added to the embryo water at 24 h post-fertilization (hpf). Handling of zebrafish was complied with the legislation of “Guangdong Laboratory Animal Management Regulations.”

NPC Xenografts and Tumor Cell Growth Quantification

Tumor cells at 85% fusion in the T25 culture flask were dissociated using 0.25% trypsin (Gibco, Thermo Fisher Scientific) and were counted before centrifugation (3,000 rpm, 3 min). Then, the supernatant was removed, and the cells were resuspended with complete medium and collected in a 1.5-ml EP tube with 3 × 10⁷ cells/ml. Tumor cells were transplanted into the perivitelline space around the yolk sac or common cardinal vein (CCV) of 2 days post-fertilization (dpf) zebrafish embryos (300–400 cells/fish) by a microinjection needle (1.0 mm × 0.6 mm) and CellTram Vario oil-pressure microinjector (Eppendorf, Hamburg, Germany); 20 zebrafish embryos were used for transplantation each group and host zebrafish were placed in an incubator at 28.5°C for 12 h, then transferred to a 34°C incubator and imaged at 3, 5, 7, and 9 dpf, respectively. Zebrafish were imaged under Leica fluorescence stereomicroscope (M205FA; Leica, Nussloch, Germany). Tumor volume was determined by quantifying the two-dimensional (2D) image area with ImageJ and the obtained areas were multiplied by the average GFP fluorescence intensity. This method has now become the standard method in the field¹⁸.

Time-Lapse Imaging of Extravasated Tumor Cells From Vessels

At 24 h post-transplantation (hpt), the larvae were imaged for NPC CNE1 cells migration by the spinning-disk confocal super resolution microscope (IXplore SpinSR; Olympus, Tokyo, Japan). Larvae were anesthetized in embryo water containing 0.02% tricaine (Sigma-Aldrich), fixed with 1% low-melting-point agarose (Thermo Fisher Scientific), and then imaged under 488 and 561 nm lasers for 11 h (every 20 min). At 48 hpt, the xenografted larvae were imaged continuously. Z projection of the confocal serial images was generated by Olympus CellSens software.

Western Blot

Cell proteins were extracted when cells grow to 100% confluence. Protein lysate (100 µl) [1 ml RIPA (radioimmunoprecipitation assay buffer) and 10 µl PMSF (phenylmethanesulfonyl fluoride); Solarbio, Beijing, China] was added to the 60-mm

culture dish (Corning, Darmstadt, Germany). Equal amounts of cellular proteins were separated with 12% SDS-PAGE (sodium dodecyl sulfate polyacrylamide gel electrophoresis) and transferred onto PVDF (polyvinylidene difluoride) membranes, which were then blocked with 5% skim milk for 2 h. Then, the PVDF membranes were incubated with primary antibodies overnight at 4°C, washed three times with TBST, followed by horseradish peroxidase (HRP)-conjugated secondary antibodies for 1 h at room temperature, and then washed three times with TBST before imaging. The primary antibodies include rabbit anti-Pin1 (ab192036; Abcam, Cambridge, UK), rabbit anti-ATF7 (ab87844, Abcam), and rabbit anti-Cyclin D1 (ab40754, Abcam). Mouse anti- β -actin (GB12001; Servicebio, Wuhan, China) and mouse anti-GAPDH (GB12002; Servicebio) were served as loading controls. Goat anti-rabbit (HS101-01; TransGen Biotech, Beijing, China) and goat anti-mouse (HS201-01; TransGen Biotech) were used as secondary antibodies. The signal bands were detected with an ECL detection kit (Thermo Fisher Scientific) and a chemiluminescence imaging system (GelView 6000M; BioLight, Xiamen, China), and the results were analyzed by ImageJ software.

Cellular Immunofluorescence

Cells were seeded in 24-well plates (2×10^5 per well) containing round glass slides (14 mm in diameter), and when cells grow to 80% confluence, the glass slides with cells on were fixed with acetone on ice for 8 min, cells were subsequently blocked with 1% bovine serum albumin (BSA) and 0.5% Tween at room temperature for 30 min, and incubated with primary antibodies overnight at 4°C. The next day, cells on the glass slides were washed three times with the block solution and incubated with fluorescent-conjugated secondary antibody for 2 h at room temperature, after which cells were washed three times with the block solution. The primary antibodies consist of mouse anti-Pin1 (sc-46660; Santa Cruz, Dallas, TX, USA), rabbit anti-Pin1 (ab192036; Abcam), rabbit anti-ATF7 (ab87844; Abcam), and rabbit anti-Cyclin D1 (ab40754; Abcam). DAPI (D9564; Sigma-Aldrich) staining was used to show the cell nucleus. Images were acquired using confocal laser scanning microscope (FV3000; Olympus) and analyzed by ImageJ software.

Immunofluorescence of Zebrafish Larvae

The method was based on a previous study¹⁹. Briefly, zebrafish larvae at 7 dpt (9 dpf of developmental stage) were fixed with 4% paraformaldehyde (PFA) at 4°C overnight. The following day, the skin of the zebrafish larvae was removed and the skinned larvae were dehydrated with methanol, then the larvae were placed in methanol at -20°C for 2 h. The dehydrated larvae were incubated with 3% H₂O₂ for 1 h at room temperature in dark. Larvae were rehydrated sequentially in

75%, 50%, and 25% methanol. Using 1% PT [1% Triton X-100 in phosphate-buffered saline (PBS)] to treat larvae four times for 15 min each. Then larvae were blocked with PBTN (4% BSA and 0.02% NaN₃ in 1% PT) at room temperature for 2 h and incubated with primary antibodies at 4°C overnight. The second day, the larvae were washed eight times with 1% PT for 30 min each and followed by incubation with fluorescent-conjugated secondary antibodies at 4°C overnight. The larvae were washed eight times with 1% PT for 30 min each. Larvae were incubated with DAPI at room temperature for 2 h, and then the larvae were washed twice with 1% PT for 30 min each. The primary antibodies include mouse anti-AE1/AE3 (ab86734; Abcam), mouse anti-Pin1 (sc-46660; SantaCruz), rabbit anti-Pin1 (ab192036; Abcam), rabbit anti-ATF7 (ab87844; Abcam), rabbit anti-Cyclin D1 (ab40754; Abcam), and goat anti-GFP (ab5450; Abcam). DAPI (D9564; Sigma-Aldrich) staining was used to show the cell nucleus. Images were acquired under confocal laser scanning microscope (FV3000; Olympus) and spinning-disk confocal super resolution microscope (IXplore SpinSR; Olympus), and analyzed with ImageJ software.

Statistical Analysis

Statistical analyses were performed by Student's *t* test, one-way analysis of variance (ANOVA) and two-way ANOVA. Statistical significance was defined as $P < 0.05$. All statistical analyses and quantitative image plotting were performed using GraphPad Prism 7 software. All data were generated and statistically analyzed from at least three independent experiments. We state that all the experiments and data are with high replicability.

Results

Establishment of Zebrafish NPC Xenograft Model

To establish zebrafish xenograft model for human NPC, we transplanted GFP-labeled human NPC CNE1 cells (Fig. 1A) into the perivitelline space around the yolk sac of 2 dpf wild-type zebrafish embryos (Fig. 1B). The xenografted zebrafish larvae were incubated at 34°C and imaged at stages of 1 dpt, 3 dpt, 5 dpt, and 7 dpt, respectively, to record and quantify the transplanted tumor cells in the fish body (Fig. 1B). Tumor cell-transplanted embryos at 1 dpt were used as controls for the comparison of tumor cell proliferation within hosts at 3 dpt, 5 dpt, and 7 dpt, respectively. As a result, the transplanted human CNE1 cells significantly increased at the stages of 5 dpt and 7 dpt compared with the number of tumor cells in fishes at 1 dpt (Fig. 1C). These suggest that human NPC CNE1 cells transplanted into zebrafish embryos could survive and proliferate well *in vivo*.

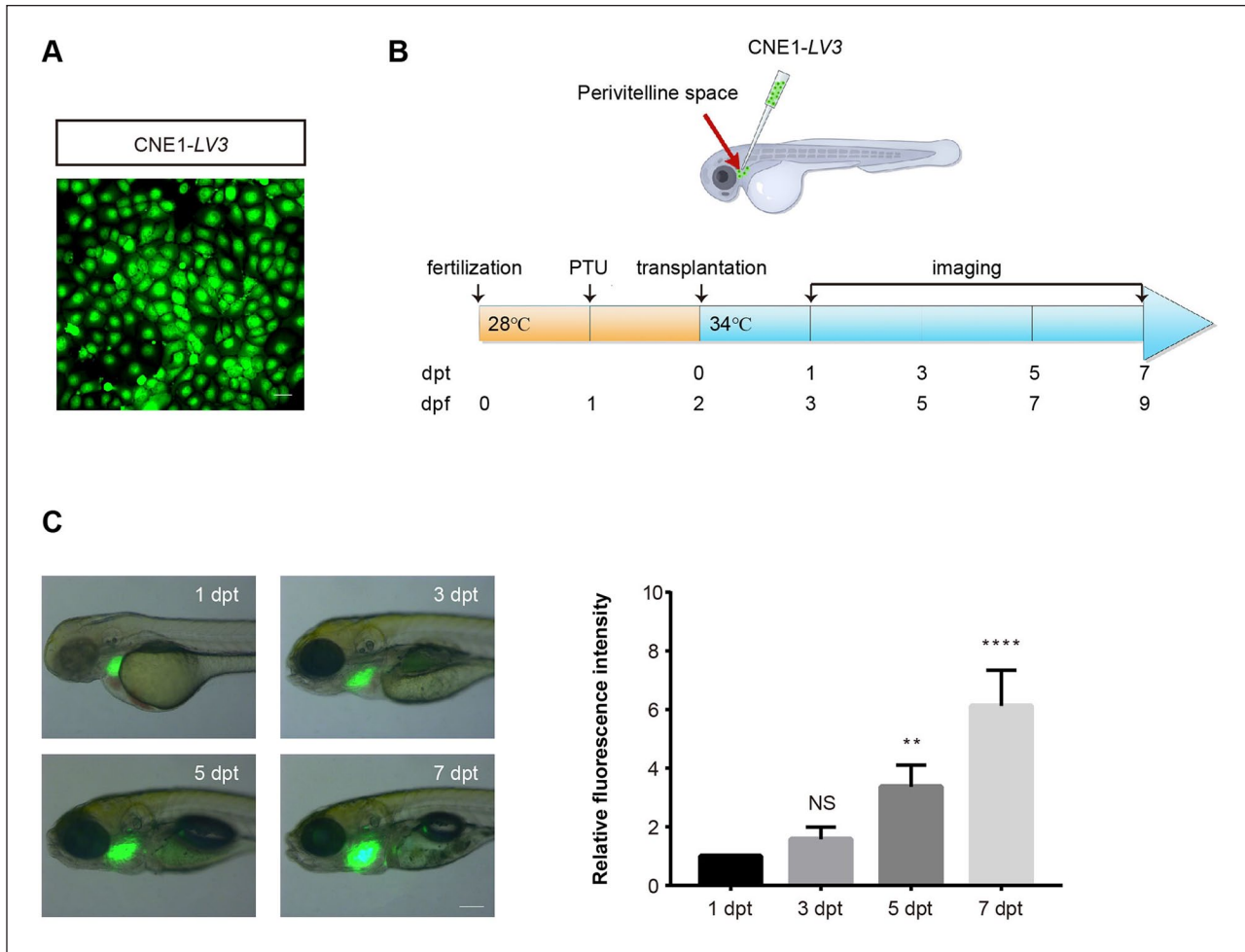


Figure 1. Xenograft of human nasopharyngeal carcinoma CNE1 cells in zebrafish. (A) Expression of GFP after transfection was detected in the stabilized cell line of CNE1 cells. Scale bar: 50 μ m. (B) Top: diagram of the establishment of zebrafish xenograft model. Bottom: experimental protocol. (C) Left: xenograft model of zebrafish at 1, 3, 5, and 7 dpt. Fluorescent and bright fields are merged, respectively. Scale bar: 1 mm. Right: the relative fluorescence intensity of tumor cells transplanted into zebrafish was quantified. The quantity of tumor cells at 1 dpt was used as the baseline, with which the quantity of tumor cells at other time points was compared. Data were quantitatively analyzed using one-way ANOVA ($n = 4$ fishes analyzed). Data are shown as mean \pm SD. GFP: green fluorescent protein; PTU: phenylthiourea; dpt: days post-transplantation; dpf: days post-fertilization; NS: not significant. ** $P < 0.01$; **** $P < 0.0001$.

Migration, Invasion, and Proliferation of Transplanted NPC CNE1 Cells in Zebrafish

Tumor metastasis is one of the main causes of death in patients, which may even occur in the early stages of tumor development when the primary tumor is relatively small²⁰. In conventional mammalian xenograft models, early-stage tumor micrometastases cannot be detected by real-time imaging analysis. In contrast, the zebrafish here provides a unique *in vivo* model that allows to visualize early micrometastases of tumor cells, and especially the invasion of cells after migrating out of the vessels. In the above assay by transplanting CNE1 cells into the perivitelline space around the embryonic yolk sac, we have observed proliferation of tumor cells in fish body. Next, to investigate the metastatic process of tumor cells in zebrafish, we transplanted tumor

cells into the CCV of 2 dpf zebrafish embryos to construct an experimental metastasis model (Fig. 2A). After transplantation of the tumor cells, embryos were incubated at 34°C and were imaged at 1, 3, 5, and 7 dpt to trace the localization of tumor cells in zebrafish circulatory system (Fig. 2A). The results showed that CNE1 cells could reach most parts of the zebrafish body, including head, trunk, and tail regions, with blood circulation (Fig. 2A). It is noteworthy that in the caudal vein plexus of the zebrafish, the migrated GFP-labeled CNE1 cells survived and proliferated with the development of the embryos (Fig. 2B). By immunofluorescence staining of tumor markers of AE1/AE3, it was found that the transplanted and migrated NPC tumor cells were tumorigenic after the extravasation from the caudal vein plexus in the tail region (Fig. 2C).

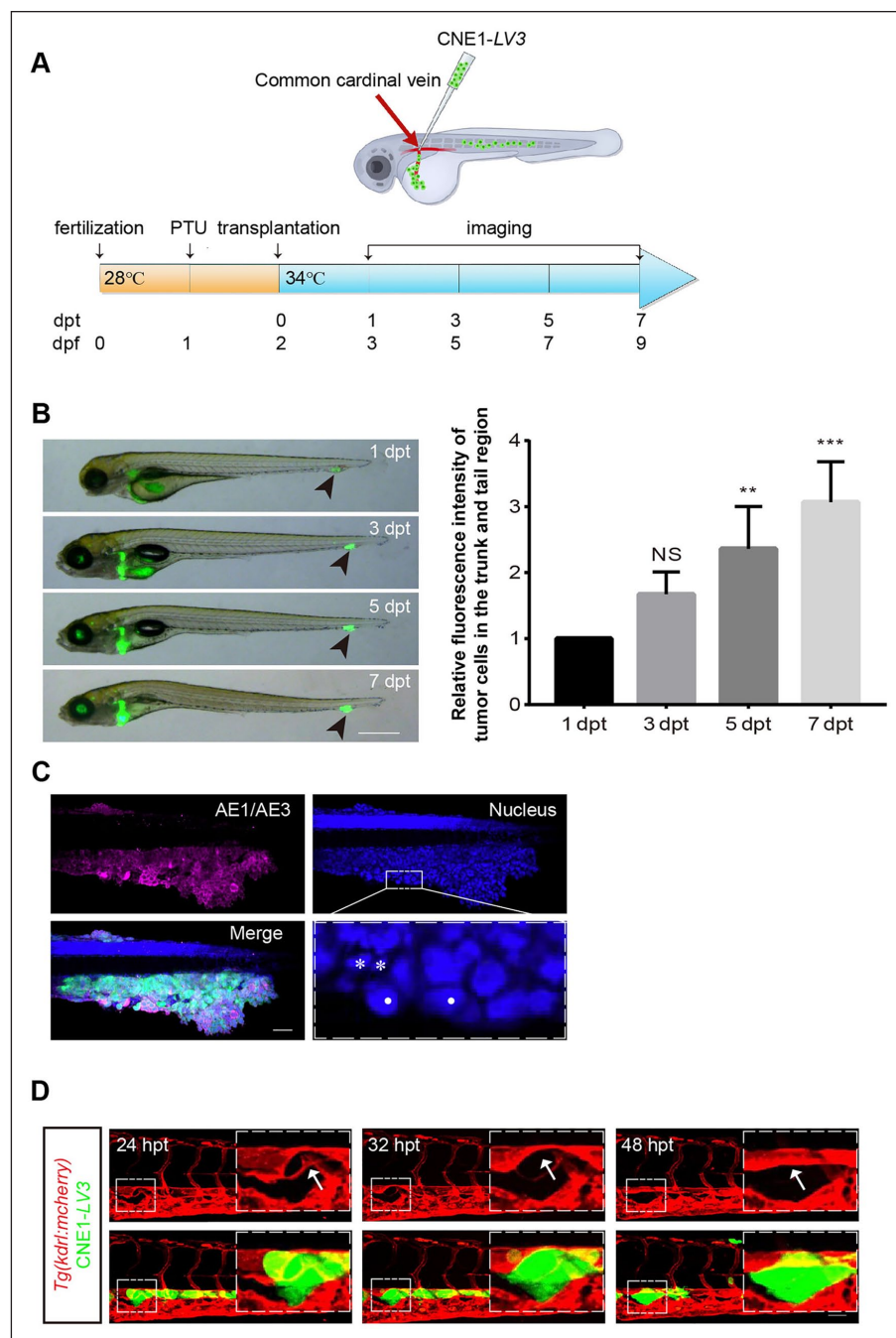


Figure 2. Transplantation of human NPC CNE1 cells into the CCV of zebrafish to observe the behavior of tumor cells. (A) Top: diagram of the establishment of zebrafish xenograft model. Bottom: experimental protocol. (B) Left: tumor cells transplanted into the circulatory system migrate to the tail region of zebrafish with blood flow and proliferated there. Black arrows indicate GFP-labeled tumor cells in the tail region. Scale bar: 3 mm. Right: the relative fluorescence intensity of tumor cells in zebrafish trunk and tail regions was quantified. The amount of tumor cells at 1 dpt was used as the baseline for comparison with that at other time points. Data were quantitatively analyzed by one-way ANOVA analysis ($n = 4$ fishes analyzed). (C) Zebrafish whole-mount immunofluorescence detection of the epithelial-derived tumor marker of AE1/AE3. Tumor cells that reached the tail region with blood flow were able to become tumorigenic in the zebrafish. Dashed line frames beneath are the high magnification of the region indicated. The nuclei of CNE1 cells are shown by white dots, and the nuclei of zebrafish are shown by white asterisks. The size of the nuclei of CNE1 cells is obviously larger than those of zebrafish. Scale bar: 50 μ m. (D) Tumor cells were transplanted into the Tg(*kdr:mCherry*) zebrafish circulatory system, and tumor cells migrated out from vessel lumen within 24–48 hpt in zebrafish tail. High magnifications of the regions (white dashed line) are shown on the right. White arrows point to the vessels (dorsal aorta) in the zebrafish. Scale bar: 50 μ m. Data are shown as mean \pm SD. NPC: Nasopharyngeal carcinoma; CCV: common cardinal vein; GFP: green fluorescent protein; PTU: phenylthiourea; dpt: days post-transplantation; dpf: days post-fertilization; hpt: hours post-transplantation; NS: not significant. ** $P < 0.01$; *** $P < 0.001$.

During the metastatic process, an important event is the invasion of cancer cells into the blood vessels to enter circulation, and later exiting the vasculature at a distant site. Therefore, we next sought to capture the migration behaviors of tumor cells out of the blood vascular wall of the caudal vein plexus by real-time images. To this end, *Tg(kdrl:mCherry)* transgenic zebrafish line which labels the vascular endothelial cells by mCherry fluorescent proteins was utilized. The results revealed that with 24 h after transplantation (from 24 to 48 hpt), CNE1 cells extravagate out from the dorsal aortic wall and invaded into intervascular space of dorsal aorta and posterior cardinal vein (Fig. 2D). Meanwhile, it was observed that the extravasation of tumor cells was accompanied by the morphological change of the vascular walls, and the arterial vessel was re-lumenized at 48 hpt when CNE1 cells completely migrated out (white arrows in Fig. 2D). The above results demonstrate that zebrafish xenograft model established can provide an ideal *in vivo* system for live tracing the processes of metastasis and invasion of tumor cells.

Knockdown of Pin1 Inhibits the Proliferation of NPC Cells

Pin1 specifically binds to and isomerizes the phosphorylated serine/threonine-proline (pSer/thro-pro) motif, leading to the alteration of protein structure, function, and stability. The structural and functional alterations of these phosphorylated proteins are closely related to the development of cancer²¹. Previous studies have shown that Pin1 is overexpressed in NPC primary tumors and tumor cell lines, and that Pin1 activates the MAPK/JNK signaling pathway and upregulates the expression level of Cyclin D1, hence inducing the growth of NPC cells²². Here, to further verify the role of Pin1 in NPC in our established zebrafish xenograft models, we constructed *Pin1*-knockdown CNE1 cell lines of NPC by transfecting *pGLV3-shPin1* plasmid which expresses green fluorescent protein (GFP). Meanwhile, the empty *pGLV3* vector-transfected CNE1 cell was used as a control. The transfected CNE1 cells were sorted by flow cytometry and imaged (Fig. 3A). Next, the expression of Pin1 was detected by western blot and immunofluorescence, respectively. The results indicated that the expression of Pin1 in the *Pin1*-knockdown cells was significantly reduced compared with that in the control group (Fig. 3B and Fig. S1A). In addition, the western blot and immunofluorescence staining of Cyclin D1 confirmed its reduced repression in *Pin1*-knockdown CNE1 cells (Fig. 3C, D).

Next, we transplanted GFP-labeled control or *Pin1*-knockdown CNE1 cells into the perivitelline space around the yolk sac of 2 dpf zebrafish embryos to investigate the survival and proliferation of these cells *in vivo* (Fig. 4A). As a result, it showed that both CNE1-*LV3* and CNE1-*shPin1* cells transplanted into the embryos could survive and proliferate within 7 dpt. However, the proliferation and growth of

Pin1-knockdown CNE1 cells were significantly inhibited when comparing with that of the control group (Fig. 4A), which is consistent with the previous reports²². To further explore the metastatic and invasive activity of CNE1 cells after knockdown of *Pin1*, we transplanted CNE1-*LV3* and CNE1-*shPin1* cells into the CCV of 2 dpf embryos, followed by real-time imaging of the xenograft embryos at 1, 3, 5, and 7 dpt, respectively (Fig. S1B). Our results revealed that due to the reduced Pin1 expression, the proliferation and invasion of CNE1-*shPin1* cells in the caudal vein plexus region of zebrafish larvae were significantly inhibited (Fig. S1B). In contrast to the transplanted CNE1-*LV3* control cells, majority of the transplanted CNE1-*shPin1* cells died out within 7 days after transplantation (white arrows in Fig. S1B). In addition, we examined the expression levels of Pin1 and Cyclin D1 in tumor cells *in vivo* after transplanted into zebrafish embryos for 7 days by immunofluorescence staining. The results indicated that the expression of both Cyclin D1 and Pin1 was reduced in *Pin1*-knockdown CNE1 cells colonized *in vivo* when compared with that in the CNE1-*LV3* cells, which was consistent with the findings of the expression of Cyclin D1 and Pin1 *in vitro* after loss of Pin1 (Fig. 4B).

The Expression Level of ATF7 Is Correlated With Pin1 in NPC

ATF7 is a member of the ATF/cAMP response element binding (CREB) protein family. Although it has already been identified for more than 20 years, its role in tumor development is still poorly understood. In contrast, the role of another ATF/CRE family member of ATF1 in NPC has already been widely explored¹⁴. Previously, we have found that both ATF7 and ATF1 strongly interacted with Pin1 by a mammalian two-hybrid assay. Therefore, we assume that Pin1 might be a potential regulatory factor of ATF7. To verify this, we analyzed the expression level of ATF7 by western blot and immunofluorescence staining after knockdown of *Pin1*, respectively. The results indicated that the expression of ATF7 was suppressed after inhibition of the expression of Pin1 (Fig. 5A and Fig. S2). To further confirm the correlation between the ATF7 and Pin1, control or *Pin1* containing plasmids were first transfected into CNE1 cells, and the expression of Pin1 and ATF7 was then analyzed by western blot. It was found that the expression of ATF7 increased significantly in *Pin1*-overexpressed CNE1 cells than that in control plasmid-transfected cells (Fig. 5B).

Subsequently, we examined the expression of ATF7 in CNE1 cells transplanted *in vivo*. The results revealed that in the inhibition of Pin1, the expression of ATF7 in CNE1-*shPin1* cells was reduced in compared with that in CNE1-*LV3* cells after transplantation in zebrafish for 7 days (Fig. 5C). Taken together, the results from *in vivo* and *in vitro* analyses suggested that Pin1 could efficiently affect the expression of ATF7, which might be also involved in Pin1-regulated carcinogenesis and development of NPC.

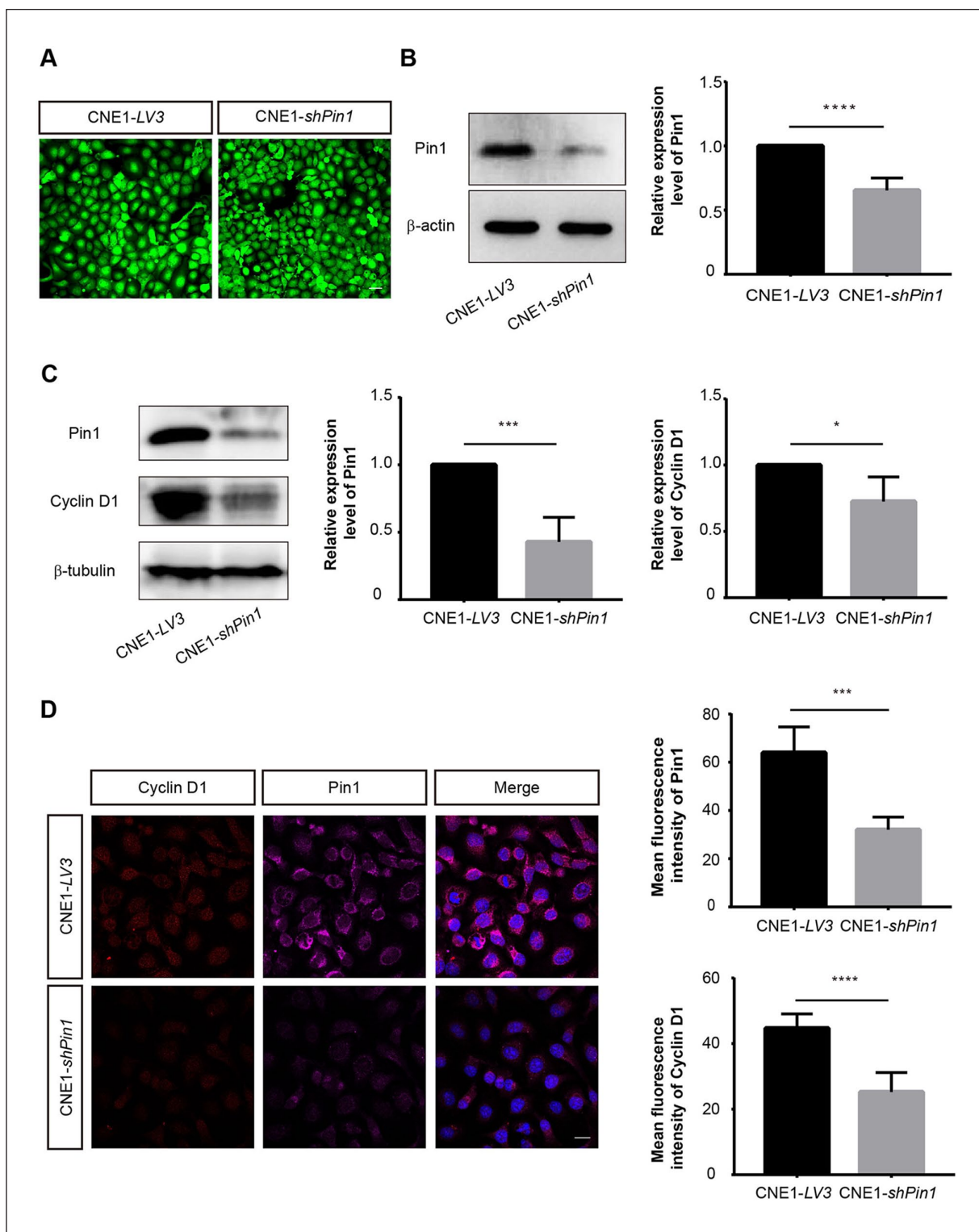


Figure 3. The expression of Cyclin D1 in tumor cells was reduced after knockdown of *Pin1*. (A) After transfection of LV3 control or *shPin1* plasmids which express GFP as selecting marker, the CNE1-LV3 and CNE1-*shPin1* cells were sorted first by FACS and imaged. Scale bar: 50 μ m. (B) Western blot analysis was performed to detect the expression of Pin1 in tumor cells. The relative expression levels of Pin1 were quantified and the data were quantitatively analyzed by Student's *t* test. Western blot (C) and immunofluorescence staining (D) of Cyclin D1 expression in CNE1 cells after knockdown of *Pin1*. Scale bar: 20 μ m. Data were quantitatively analyzed using Student's *t* test. Data are shown as mean \pm SD. GFP: green fluorescent protein; FACS: fluorescence activating cell sorter. **P* < 0.05; ***P* < 0.001; ****P* < 0.0001.

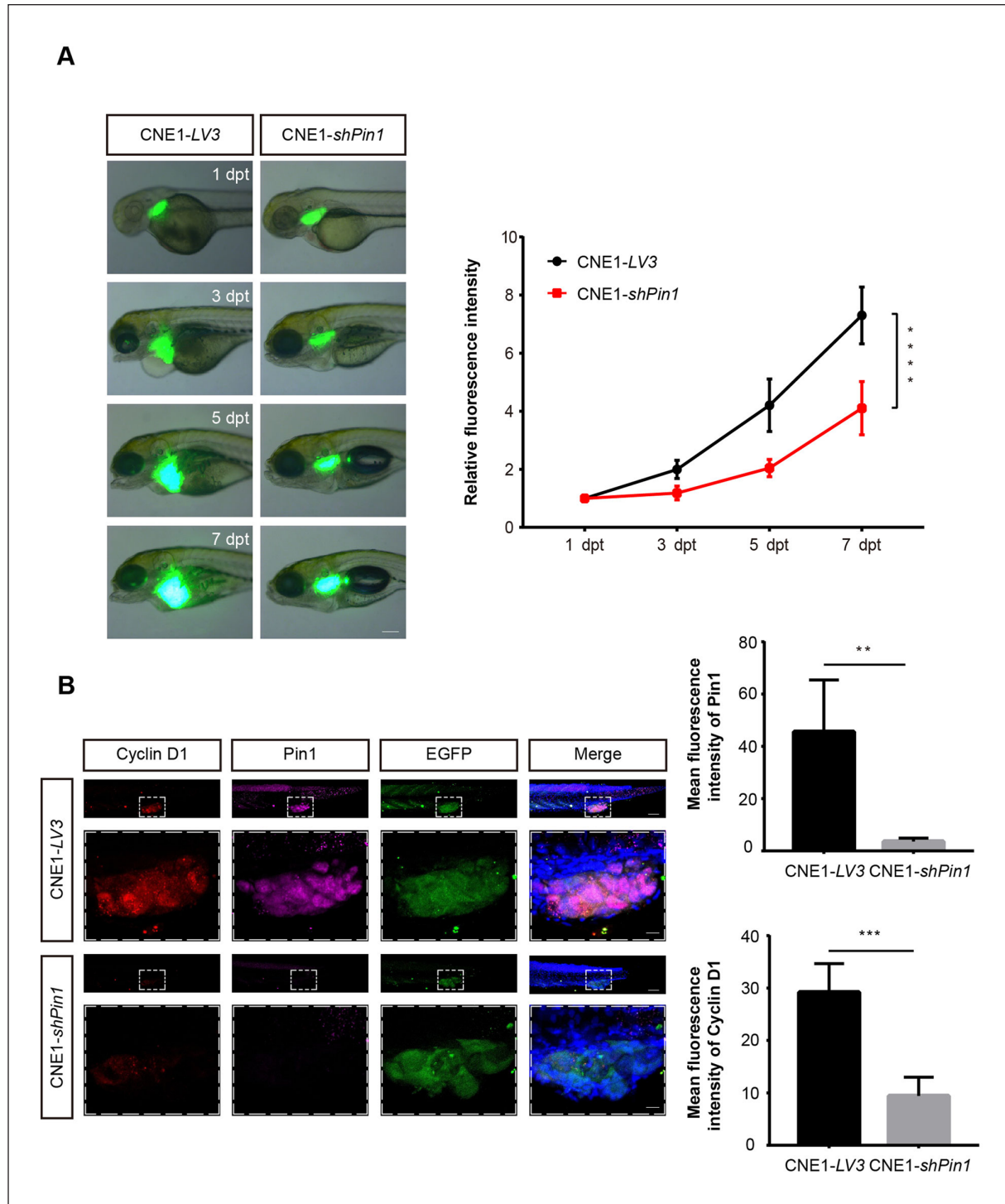


Figure 4. Inhibition of Pin1 expression suppressed tumor cell proliferation in zebrafish. (A) Combined fluorescence and bright field images of zebrafish xenograft model transplanted with CNE1-LV3 or CNE1-*shPin1* into the perivitelline space around the yolk sac at 1, 3, 5, and 7 dpt, respectively. The relative fluorescence intensity of the tumor cells in zebrafish was quantified. The amount of tumor cells at 1 dpt was used as the baseline with which the amount of tumor cells at other time points was compared. The differences in cell proliferation between the two groups were quantitatively analyzed by two-way ANOVA (CNE1-LV3 group, $n = 6$ transplanted fishes analyzed; CNE1-*shPin1* group, $n = 11$ transplanted fishes analyzed). Scale bar: 1 mm. (B) Whole-mount embryo immunofluorescence staining of Pin1 and Cyclin D1 expression in zebrafish with tumor cells transplanted at 7 dpt. Selected areas of images (white dashed line) are shown with a higher magnification below. Scale bar: 50 μm ; 10 μm in the amplified image. The mean fluorescence intensity of Pin1 and Cyclin D1 was quantitatively measured, and the data were quantitatively analyzed by Student's *t* test (CNE1-LV3 group, $n = 6$ transplanted fishes analyzed; CNE1-*shPin1* group, $n = 4$ transplanted fishes analyzed). Data are shown as mean \pm SD. dpt: days post-transplantation; EGFP: enhanced green fluorescent protein. ** $P < 0.01$; *** $P < 0.001$; **** $P < 0.0001$.

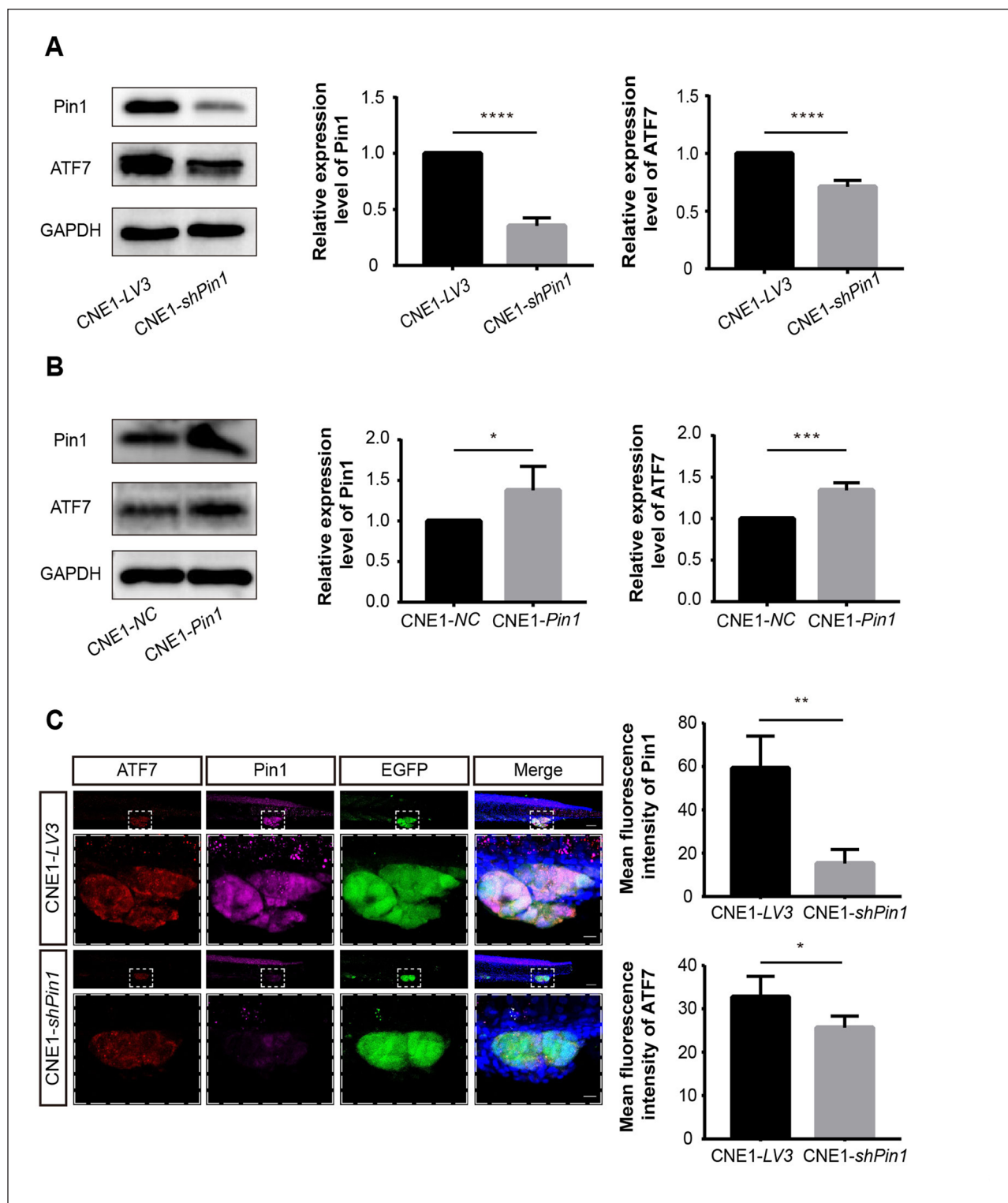


Figure 5. The expression of ATF7 was correlated with the expression of Pin1. (A-B) Western blot analysis was used to detect the expression of ATF7 in *Pin1*-knockdown or *Pin1*-overexpressed CNE1 cells. The relative expression levels of Pin1 and ATF7 were quantified ($n = 4$ independent repeats). (C) Whole-mount embryo immunofluorescence staining of ATF7 expression in tumor cells transplanted in zebrafish. Images of selected areas (white dashed line) are shown at higher magnification below. Scale bar: 50 μm ; 10 μm in the amplified image. The mean fluorescence intensity of Pin1 and ATF7 was analyzed quantitatively. The data were quantitatively analyzed by Student's *t* test (CNE1-LV3 group, $n = 5$ transplanted fishes analyzed; CNE1-shPin1 group, $n = 3$ transplanted fishes analyzed). Data are shown as mean \pm SD. GAPDH: glyceraldehyde-3-phosphate dehydrogenase; EGFP: enhanced green fluorescent protein. * $P < 0.05$; ** $P < 0.01$; *** $P < 0.001$; **** $P < 0.0001$.

In summary, our data provide strong evidences that zebrafish could provide a simple, rapid, and visual xenograft model that allows for human cancer research compared with traditional rodent models.

Discussion

Although the combination of chemotherapy and radiotherapy has contributed to the increased survival rate of the NPC patients (5-year survival rate around 85% to 90%)^{3,4}, distant metastasis, recurrence, and chemoresistance are still challenges in the treatment for NPC. Therefore, studies on pathogenesis of NPC, identification of NPC-related biomarkers, optimization of treatment strategies for different patients, and development of novel treatment methods are urgently needed. In the traditional *in vitro* tumor models, analysis of the interaction between tumor and host is hardly possible for the study of behavior and complexity of tumor, which are essential events in tumor growth and progression. Therefore, translational studies using *in vitro* model for clinical application are still challenging²³, and to develop more efficient *in vivo* models will help to explore accurate therapeutic strategies for cancer patients. In this study, we established a xenograft NPC model using classic model animal of zebrafish and confirmed that human NPC cells can survive and proliferate in zebrafish embryos. In addition, we combined the perivitel-line space transplantation with the CCV transplantation and observed the extravasation behaviors of NPC cells out of the blood vessels for the first time. We proved that human tumor cells can proliferate, migrate, and invade in zebrafish body. Based on these observations, we propose that the zebrafish xenograft model enables to visualize and investigate NPC cell metastasis *in vivo*.

Pin1 is a key signal-regulating protein in tumors, which is highly expressed in invasive tumors, and is closely related to the development and prognosis of tumors²⁴⁻²⁶. Existing studies have confirmed that Pin1 is involved in the occurrence and development of NPC^{14,24}. As a downstream gene of multiple signaling pathways, *Cyclin D1* mainly plays a role in the process of G1 phase entering to S phase of cell cycle and has important influence on cell growth related to tumor deterioration and metastasis²⁷. In breast cancer, Pin1 overexpression is associated with increased expression of Cyclin D1²⁸. In hepatocellular carcinoma, Pin1 overexpression has also been shown to upregulate Cyclin D1²⁹. In NPC, overexpression of Pin1 activates MAPK/JNK and NF- κ B pathway, thereby regulating the expression of Cyclin D1²². In this study, to evaluate the feasibility of zebrafish NPC xenograft model for tumor studies, we verified the regulatory effect of Pin1 on Cyclin D1 expression in transplanted CNE1 cell in zebrafish. The finding was in consistent with those obtained *in vitro* and in mice that loss of Pin1 inhibits the expression of Cyclin D1 thus inhibiting the proliferation of NPC cells²².

ATF7 is a member of CREB protein family, and many members of the ATF/CREB family are associated with cancer

progression. For example, ATF1 promotes the invasiveness of thyroid papillary tumors³⁰, ATF3 promotes the invasiveness of prostate tumor cells³¹, and overexpression of ATF4 leads to drug resistance in human cancer cell lines³². It has been demonstrated that ATF7 expression is upregulated in hepatocellular carcinoma tissues and that inhibition of ATF7 expression inhibits hepatocellular carcinoma cell proliferation and promotes apoptosis³³. However, the role of ATF7 in NPC has not yet been reported. In this study, we found that the expression of ATF7 in NPC cells was correlated with that of Pin1. Therefore, we hypothesized that Pin1 might be a new regulator of ATF7, and Pin1 might function in promoting the development of NPC by regulating the expression of ATF7. However, the mechanism of the regulation of Pin1 on ATF7 has not been clarified, and the mechanism of ATF7 in NPC development needs to be further explored.

Although many advantages make zebrafish a suitable *in vivo* model for cancer research, there are still some inherent disadvantages, such as the different incubation temperatures for zebrafish and mammalian cells, and diverse tumor microenvironment. Regarding the culturing temperature, the optimal growth temperature for human tumor cells is 37°C, whereas it is 28°C for zebrafish. Therefore, the incubation temperature of 34°C was tested and finally chosen as the compromise temperature in our study. This temperature may lead to changes of zebrafish metabolism³⁴. Nevertheless, the zebrafish xenograft model in our study provides an intact microenvironment close to that in humans for tumor growth. In addition, the unique imaging advantages of transparent fish bodies, combining with multiple transgenic labeling of various organs, allow us to real-timely record the behaviors of tumor cells for a long period (7 days after tumor cell transplantation). In summary, we established a zebrafish xenograft NPC model and briefly verified the involvement of ATF7 regulated by Pin1 in the occurrence of NPC.

Conclusion

The zebrafish xenograft model provides an ideal *in vivo* system for rapid identification of tumor formation and progressing and efficiently contributes to explore the mechanisms of NPC carcinogenesis and development.

Acknowledgments

We thank Yuezhuang Zheng and Qiumei Hong for expert technical assistance with the fish facility and also we thank the Public Service Platform of South China Sea for the R&D of Marine Biomedicine Resource for support.

Author Contributions

E.H. performed the experiments, analyzed the data, and drafted the manuscript. H.H. and L.W. help with the cell experiment and transplantation. B.L. generated the stabilized cells. Z.H. gave suggestions and guidance. J.Z. initiated this study and monitored the whole progress of this project.

Ethical Approval

The whole experimental procedures were examined by the Clinical Ethics Committee of the Affiliated Hospital of Guangdong Medical University, China.

Statement of Human and Animal Rights

This study does not contain any studies with human subjects or with rodent vertebrates. Handling of zebrafish was performed in accordance with Guangdong State Regulations on Laboratory Animal Management (2010).

Statement of Informed Consent

Not applicable.

Declaration of Conflicting Interests

The author(s) declared no potential conflicts of interest with respect to the research, authorship, and/or publication of this article.

Funding

The author(s) disclosed receipt of the following financial support for the research, authorship, and/or publication of this article: This work was supported by the National Natural Science Foundation of China (31970777, 81372137) and Discipline Construction Project of Guangdong Medical University (4SG22258G).

ORCID iD

Jingjing Zhang  <https://orcid.org/0000-0002-8789-4638>

Supplemental Material

Supplemental material for this article is available online.

References

- Bray F, Ferlay J, Soerjomataram I, Siegel RL, Torre LA, Jemal A. Global cancer statistics 2018: GLOBOCAN estimates of incidence and mortality worldwide for 36 cancers in 185 countries. *CA Cancer J Clin*. 2018;68(6):394–424.
- Chen YP, Chan AT, Le QT, Blanchard P, Sun Y, Ma J. Nasopharyngeal carcinoma. *Lancet*. 2019;394(10192):64–80.
- Blanchard P, Lee A, Marguet S, Leclercq J, Ng WT, Ma J, Chan AT, Huang PY, Benhamou E, Zhu G, Chua DT, et al. Chemotherapy and radiotherapy in nasopharyngeal carcinoma: an update of the MAC-NPC meta-analysis. *Lancet Oncol*. 2015;16(6):645–55.
- Perri F, Della Vittoria Scarpato G, Buonerba C, Di Lorenzo G, Longo F, Muto P, Schiavone C, Sandomenico F, Caponigro F. Combined chemo-radiotherapy in locally advanced nasopharyngeal carcinomas. *World J Clin Oncol*. 2013;4(2):47–51.
- Geara FB, Glisson BS, Sanguineti G, Tucker SL, Garden AS, Ang KK, Lippman SM, Clayman GL, Goepfert H, Peters LJ, Hong WK. Induction chemotherapy followed by radiotherapy versus radiotherapy alone in patients with advanced nasopharyngeal carcinoma: results of a matched cohort study. *Cancer*. 1997;79(7):1279–86.
- Perri F, Bosso D, Buonerba C, Lorenzo GD, Scarpato GD. Locally advanced nasopharyngeal carcinoma: current and emerging treatment strategies. *World J Clin Oncol*. 2011;2(12): 377–83.
- Ito M, Hiramatsu H, Kobayashi K, Suzue K, Kawahata M, Hioki K, Ueyama Y, Koyanagi Y, Sugamura K, Tsuji K, Heike T, et al. NOD/SCID/gamma(c)(null) mouse: an excellent recipient mouse model for engraftment of human cells. *Blood*. 2002;100(9):3175–82.
- Howe K, Clark MD, Torroja CF, Torrance J, Berthelot C, Muffato M, Collins JE, Humphray S, McLaren K, Matthews L, McLaren S, et al. The zebrafish reference genome sequence and its relationship to the human genome. *Nature*. 2013;496(7446): 498–503.
- Outtandy P, Russell C, Kleta R, Bockenbauer D. Zebrafish as a model for kidney function and disease. *Pediatr Nephrol*. 2019;34(5):751–62.
- Fazio M, Ablain J, Chuan Y, Langenau DM, Zon LI. Zebrafish patient avatars in cancer biology and precision cancer therapy. *Nat Rev Cancer*. 2020;20(5):263–73.
- Lieschke GJ, Trede NS. Fish immunology. *Curr Biol*. 2009; 19(16):R678–82.
- Lam SH, Chua HL, Gong Z, Lam TJ, Sin YM. Development and maturation of the immune system in zebrafish, *Danio rerio*: a gene expression profiling, in situ hybridization and immunological study. *Dev Comp Immunol*. 2004;28(1):9–28.
- Zon LI, Peterson RT. In vivo drug discovery in the zebrafish. *Nat Rev Drug Discov*. 2005;4(1):35–44.
- Huang GL, Liao D, Chen H, Lu Y, Chen L, Li H, Li B, Liu W, Ye C, Li T, Zhu Z, et al. The protein level and transcription activity of activating transcription factor 1 is regulated by prolyl isomerase Pin1 in nasopharyngeal carcinoma progression. *Cell Death Dis*. 2016;7(12):e2571.
- Kimmel CB, Ballard WW, Kimmel SR, Ullmann B, Schilling TF. Stages of embryonic development of the zebrafish. *Dev Dyn*. 1995;203(3):253–310.
- Westerfield M. The zebrafish book: a guide for the laboratory use of zebrafish (*Danio rerio*). 4th ed. Eugene (OR): University of Oregon; 2000.
- Wrobel JK, Najafi S, Ayhan S, Gatzweiler C, Kronic D, Ridinger J, Milde T, Westermann F, Peterziel H, Meder B, Distel M, et al. Rapid in vivo validation of HDAC inhibitor-based treatments in neuroblastoma zebrafish xenografts. *Pharmaceuticals (Basel)*. 2020;13(11):345.
- Yan C, Brunson DC, Tang Q, Do D, Iftimia NA, Moore JC, Hayes MN, Welker AM, Garcia EG, Dubash TD, Hong X, et al. Visualizing engrafted human cancer and therapy responses in immunodeficient zebrafish. *Cell*. 2019;177(7): 1903–14.e14.
- He J, Mo D, Chen J, Luo L. Combined whole-mount fluorescence in situ hybridization and antibody staining in zebrafish embryos and larvae. *Nat Protoc*. 2020;15(10):3361–79.
- Rouhi P, Jensen LD, Cao Z, Hosaka K, Lanne T, Wahlberg E, Steffensen JF, Cao Y. Hypoxia-induced metastasis model in embryonic zebrafish. *Nat Protoc*. 2010;5(12):1911–18.
- Yu JH, Im CY, Min SH. Function of PIN1 in cancer development and its inhibitors as cancer therapeutics. *Front Cell Dev Biol*. 2020;8:120.
- Xu M, Cheung CC, Chow C, Lun SW, Cheung ST, Lo KW. Overexpression of PIN1 enhances cancer growth and aggressiveness with cyclin d1 induction in EBV-associated nasopharyngeal carcinoma. *PLoS ONE*. 2016;11(6):e0156833.
- Sounni NE, Noel A. Targeting the tumor microenvironment for cancer therapy. *Clin Chem*. 2013;59(1):85–93.

24. Zeng L, Luo S, Li X, Lu M, Li H, Li T, Wang G, Lyu X, Jia W, Dong Z, Jiang Q, et al. Functional PIN1 promoter polymorphisms associated with risk of nasopharyngeal carcinoma in Southern Chinese populations. *Sci Rep.* 2017;7(1):4593.
25. Jiang L, Cao M, Hu J, Chen J. Expression of PIN1 in gastrointestinal stromal tumours and its clinical significance. *Anticancer Res.* 2016;36(3):1275–80.
26. Jiang L, Chu H, Zheng H. Pin1 is related with clinical stage of papillary thyroid carcinoma. *World J Surg Oncol.* 2016;14:95.
27. Yan W, Cheng L, Zhang D. Ultrasound-targeted microbubble destruction mediated si-CyclinD1 inhibits the development of hepatocellular carcinoma via suppression of PI3K/AKT signaling pathway. *Cancer Manag Res.* 2020;12:10829–39.
28. Wulf GM, Ryo A, Wulf GG, Lee SW, Niu T, Petkova V, Lu KP. Pin1 is overexpressed in breast cancer and cooperates with Ras signaling in increasing the transcriptional activity of c-Jun towards cyclin D1. *EMBO J.* 2001;20(13):3459–72.
29. Pang RW, Lee TK, Man K, Poon RT, Fan ST, Kwong YL, Tse E. PIN1 expression contributes to hepatic carcinogenesis. *J Pathol.* 2006;210(1):19–25.
30. Leslie MC, Bar-Eli M. Regulation of gene expression in melanoma: new approaches for treatment. *J Cell Biochem.* 2005;94(1):25–38.
31. Bandyopadhyay S, Wang Y, Zhan R, Pai SK, Watabe M, Iizumi M, Furuta E, Mohanta S, Liu W, Hirota S, Hosobe S, et al. The tumor metastasis suppressor gene Drg-1 down-regulates the expression of activating transcription factor 3 in prostate cancer. *Cancer Res.* 2006;66(24):11983–90.
32. Igarashi T, Izumi H, Uchiumi T, Nishio K, Arao T, Tanabe M, Uramoto H, Sugio K, Yasumoto K, Sasaguri Y, Wang KY, et al. Clock and ATF4 transcription system regulates drug resistance in human cancer cell lines. *Oncogene.* 2007;26(33):4749–60.
33. Song F, Wei M, Wang J, Liu Y, Guo M, Li X, Luo J, Zhou J, Wang M, Guo D, Chen L, et al. Hepatitis B virus-regulated growth of liver cancer cells occurs through the microRNA-340-5p-activating transcription factor 7-heat shock protein A member 1B axis. *Cancer Sci.* 2019;110(5):1633–43.
34. Long Y, Li L, Li Q, He X, Cui Z. Transcriptomic characterization of temperature stress responses in larval zebrafish. *PLoS ONE.* 2012;7(5):e37209.